scientific reports

Check for updates

OPEN

Simulation study of the influence of circular arc vortex generator size on the heat transfer characteristics of fin-and-tube heat exchanger

Xuejun Qi[1]✉, Jingrong Yang[1], Yong Zhang[2], Jingjing Wang[1] & Xinyu Guo[1]

Vortex generators (VGs) are extensively utilized in refrigeration equipment to enhance heat transfer performance. This study investigates the geometric optimization of circular arc VGs for improving the thermal performance of fin-and-tube heat exchangers (FTHEs) through numerical simulations. Key geometric parameters (central angle (θ), height (H), inclination angle (α), and attack angle (β)) were systematically analyzed to evaluate their effects on the heat transfer factor (j), friction factor (f), and thermal performance factor (JF). Simulations conducted via ANSYS Fluent 2021R1 revealed that increasing θ enhances vorticity and heat transfer efficiency, with JF rising by 5.2% at θ = 35°. An optimal height of H ≥ 0.8 mm was identified, achieving a 13.0% improvement in j at H = 1.6 mm. While inclination angles below 35° demonstrated minimal impact, inclination angles exceeding 35° significantly intensified turbulent mixing, resulting in an 8.2% increase in j at α = 50°. Higher β value is beneficial to enhance convective heat transfer, achieving 2.0% improvements in JF at β = 30°. This study highlights the critical importance of VG size in optimizing the balance between heat transfer enhancement and pressure loss. These findings offer practical insights for designing energy-efficient FTHEs and advancing sustainable refrigeration technologies.

Keywords Fin-and-tube heat exchanger, Circular arc vortex generator, Numerical simulation, Heat transfer enhancement, Computational fluid dynamics

Abbreviations

A	Heat transfer area (m^2)
c_p	Specific heat capacity (J/(kg · K)
D_c	Outer diameter of tube (mm)
e	Relative error
f	Friction factor
F_P	Fin spacing (mm)
H	Height (mm)
h	Convective heat transfer coefficient (W/(m^2 · K))
j	Heat transfer factor
JF	Thermal performance factor
m	Mass flow rate of air (kg/s)
L	Length (m)
Nu	Nusselt number
P	Order of accuracy of GCI
r	Grid refinement ratio
Re	Reynolds number
S_1	Row spacing (mm)
S_2	Tube spacing (mm)
Pr	Prandtl number
Q	Heat transfer capacity (W)
VG	Vortex generator
V	Airflow velocity

[1]School of Architecture and Civil Engineering, Xihua University, Chengdu 610039, China. [2]Sichuan Yibai Refrigeration Equipment Co., Ltd, Chengdu 610511, China. ✉email: xuejunqi@foxmail.com

T	Temperature (K)
u, v, w	Velocity vector (m/s)
u_m	Airflow velocity at the narrowest point (m/s)
x, y, z	Coordinates
Δp	Pressure drop (Pa)
ΔT	Logarithmic mean temperature difference (K)

Greek symbols

α	Inclination angle (°)
β	Attack angle (°)
θ	Central angle (°)
λ	Thermal conductivity of air (W/(m · K))
μ	Viscosity (kg/(m · s))
ρ	Density (kg/m^3)
ϕ	Numerical solution
δ_f	Fin thickness (mm)

Subscripts

in	Inlet
out	Outlet
w	Wall

The implementation of fin-and-tube heat exchangers (FTHEs) in refrigeration systems represents an essential component for enhancing heat transfer efficiency. The incorporation of fins on tube surfaces significantly improves air side heat transfer efficiency[1], enabling heat exchangers to achieve superior thermal performance within compact spatial constraints. With ongoing technological advancements and industrial development, the application range of FTHEs continues to expand across various refrigeration domains.

Numerous researchers have conducted comprehensive investigations into the geometric configuration, dimensional parameters, material selection, heat exchange tubes, and structural arrangement of FTHEs[2–4]. Due to the inherent low thermal conductivity of air, the air side thermal resistance constitutes the dominant resistance in the heat transfer process[5]. Consequently, augmenting air side heat transfer represents a crucial strategy for optimizing FTHEs thermal performance. Kang et al.[6] experimentally demonstrated that slotted fins exhibit a significantly higher Nusselt number (Nu) compared to conventional fin in FTHEs applications. Ouyang et al.[7] revealed through comparative analysis that equidistant corrugated finned tubes demonstrate superior heat transfer characteristics relative to staggered corrugated configurations. Habibian et al.[8] performed a systematic comparison between conventional fins and louvered fins, documenting a 24.6% enhancement in heat transfer rate accompanied by a 67.7% increase in air side pressure drop for louvered fin configurations.

Johnson et al.[9] proposed installing VGs in heat exchanger channels to enhance thermal performance. Fiebig et al.[10] concluded that longitudinal vortices enhance heat transfer more effectively than transverse vortices. Modi et al.[11] reported that rectangular-winglet VGs in FTHEs demonstrate a superior heat transfer coefficient compared to non-VG configurations. Han et al.[12] found that perforated rectangular VGs exhibit enhanced heat transfer performance relative to their solid counterparts. Leu et al.[13] investigated the influence of attack angle on the efficiency of FTHEs, demonstrating an 8% improvement in thermal performance when reducing the attack angle from 60° to 45°. Allison and Dally[14] examined triangular VGs, observing an 87% increase in heat transfer capacity compared to the FTHE without VGs. Lotfi et al.[15] conducted comparative analyses of rectangular-trapezoidal, angular-rectangular, and curved-rectangular winglets, revealing that curved-angled rectangular configurations achieve optimal thermal performance at Reynolds numbers (Re) ranging from 500 to 3,000. Zheng et al.[16] developed trapezoidal cross-section longitudinal VGs, demonstrating their superior thermal performance over rectangular-section designs.

With the progress in research, scholars have increasingly focused on curved VGs[17]. Zhou and Ye[18] performed experimental studies on curved trapezoidal winglets, demonstrating enhanced heat transfer performance at smaller attack angles and larger inclination angles. Esmaeilzadeh et al.[19] compared trapezoidal winglets with curved trapezoidal winglets, revealing lower pressure drop and superior overall performance in curved configurations. Song et al.[20] investigated delta winglet VGs, reporting a 18.79% increase in $j/f^{1/3}$ compared to conventional FTHEs designs.

In studies of circular arc VGs, prior research has extensively investigated the effects of position, radial distance, and surface curvature on VGs performance[21,22]. However, the influence of circular arc VGs dimensions on the heat transfer characteristics of FTHEs remains insufficiently explored. To address this research gap, the present study systematically examines how geometric parameters of circular arc VGs affect the thermal performance and flow characteristics in FTHEs. We first investigate the variation of temperature and velocity fields induced by circular arc VGs within the FTHE configuration. Subsequently, we conduct parametric analyses to evaluate the effects of key geometric parameters: height (H), central angle (θ), inclination angle (α), and attack angle (β) on FTHEs performance. This research not only provides insights for optimizing heat exchanger design but also contributes to sustainability initiatives through enhanced energy efficiency.

Numerical simulation details

Physical model

Figure 1 shows the FTHE with circular arc VGs. The copper tubes are arranged in a fork row configuration. Table 1 summarizes the key geometrical parameters of the FTHEs. Air enters the inlet at a prescribed velocity, undergoes heat exchange with the FTHEs, and exits through the outlet, while refrigerant circulates through the copper tubes. Circular arc VGs are primarily located in the wake region downstream of the copper tubes[23,24].

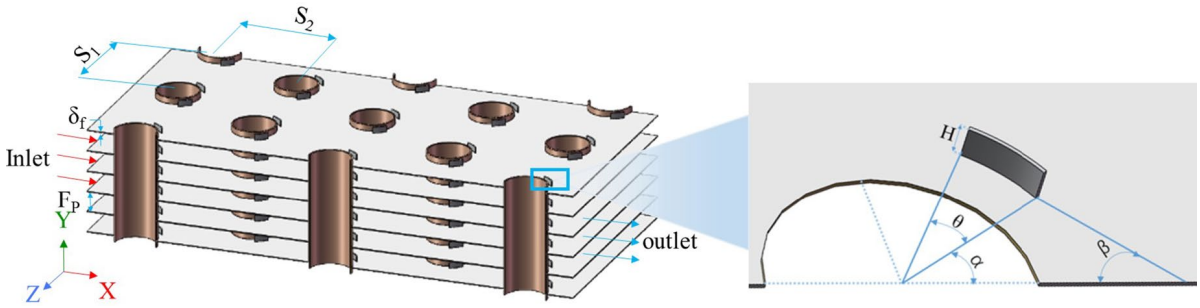

Fig. 1. Schematic of FTHE with circular arc VGs.

	Value (mm)
Fin thickness (δ_f)	0.15
Fin spacing (F_p)	4.00
Outer diameter of copper tube (D_c)	9.52
Row spacing (S_1)	25.00
Tube spacing (S_2)	21.65

Table 1. The key geometrical parameters of the FTHEs.

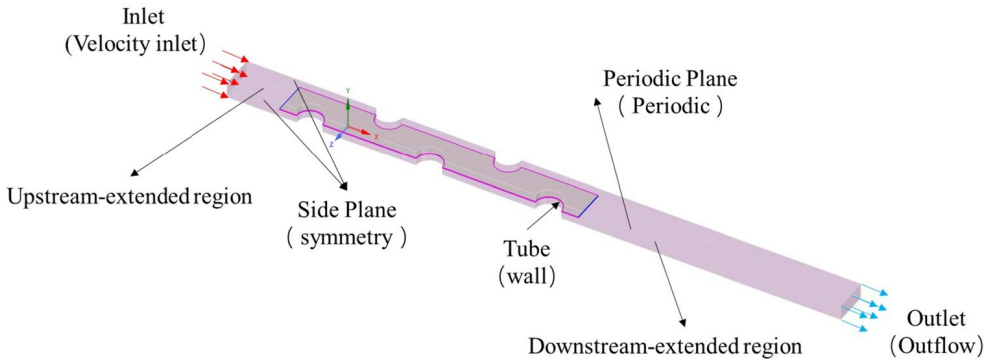

Fig. 2. Calculation region and boundary conditions.

	Materials	Density (kg/m^3)	Specific heat capacity (J/(kg · K))	Thermal conductivity (W/(m · K))
Air	–	1.225	1006.43	0.0242
Fins /VGs	Aluminum	2719	871	202.4
Circular tube	Copper	8978	381	387.6

Table 2. The properties of materials.

When airflow passes through the VGs, it induces longitudinal vortices that generate turbulent flow near the copper tube surfaces. This configuration significantly increases the heat transfer coefficient while improving air side thermal performance[25].

Calculation domain and simulation parameter setting

The FTHEs configuration is simplified in this study, with geometric complexity and symmetry systematically considered. Figure 2 illustrates the computational domain consisting of fluid and solid regions. The coordinate system is defined with the X-axis aligned with airflow direction, Y-axis with fin thickness, and Z-axis with the longitudinal fin dimension. To ensure uniform inlet velocity distribution and prevent outlet backflow, flow domains were extended with the inlet maintained at twice the tube diameter and outlet at tenfold the tube diameter[26]. This differential extension promotes boundary layer development while suppressing airflow recirculation. The properties of materials are summarized in Table 2.

The inlet boundary was defined as a velocity-inlet with uniform velocity and temperature[27]. The inlet temperature was set to 308 K. The outlet was set as the free flow. Given the copper tubes' high thermal conductivity and surface heat transfer coefficient, their wall temperature was fixed at 285 K[28]. Symmetric boundary conditions were applied to front/rear boundaries along the Z-axis (computational-domain sides and fin edges). Upper/lower Y-axis boundaries (domain top/bottom surfaces) were defined as periodic boundaries. Fluid-solid interfaces were defined at all air/solid contact surfaces within the computational domain. The boundary condition equations are listed in Table 3.

Numerical simulations were performed using ANSYS Fluent 2021R1. The Re number range of the fluid is between 2,038 and 6,037. k-ω turbulence model was adopted for the calculation, and the SIMPLEC algorithm was used to couple the pressure field and velocity field[29]. The enhanced wall treatment was adopted as the near-wall function, whereby the first layer grid height was used to satisfy $y+\approx 1$. Convection and diffusion terms were discretized using a second-order upwind scheme. Convergence criteria were set as follows: the residual of the momentum equation was 10^{-8}, and the residual of other equations was 10^{-6}. The sub-relaxation factors for pressure, momentum, and energy were set to 0.3, 0.7, and 1, respectively.

Governing equations

The numerical simulation adopts the following assumptions:

(1) Airflow is three-dimensional and incompressible;
(2) Gravity, buoyancy, and thermal radiation are neglected;
(3) Heat transfer is considered exclusively, with mass transfer excluded.

Under these assumptions, the governing equations are formulated as follows:

$$\text{Continuity equation}: \frac{\partial \rho \mathrm{ui}}{\partial \mathrm{xi}} = 0, (\mathrm{i} = 1, 2, 3) \tag{1}$$

$$\text{Momentum equation}: \frac{\partial(\rho \mathrm{ui} uj)}{\partial xi} = -\frac{\partial p}{\partial xi} + \frac{\partial}{\partial xi}(\mu \frac{\partial ui}{\partial xi} - \rho \overline{u_i' u_j'}), (i = j = 1, 2, 3; i \neq j) \tag{2}$$

$$\text{Energy equation}: \rho cpui \frac{\partial T}{\partial xi} = \frac{\partial}{\partial xi}(\lambda \frac{\partial T}{\partial xi}), (i = j = 1, 2, 3) \tag{3}$$

where ρ denotes the density of air (kg/m^3), μ denotes dynamic viscosity (Pa·s), c_p represents the specific heat capacity of air (J/(kg · K)), and λ indicates the thermal conductivity of air (W/(m · K)).

Data processing

Reynolds number[30]:

$$\mathrm{Re\,Dc} = \frac{\rho \mathrm{umDc}}{\mu} \tag{4}$$

where u_m denotes the airflow velocity at the narrowest point of the channel (m/s), and Dc represents the outer diameter of the copper tube (m).

Nusselt number[30]:

$$\mathrm{Nu} = \frac{\mathrm{hDc}}{\lambda} \tag{5}$$

$$\mathrm{h} = \frac{\mathrm{Q}}{\mathrm{A0}\Delta \mathrm{T}} \tag{6}$$

where h denotes the convective heat transfer coefficient (W/(m^2 · K)), A_0 denotes the heat transfer area (m^2), Q represents the heat transfer capacity of FTHE (W), and ΔT represents the logarithmic mean temperature difference (K).

The calculation formula of Q[31]:

$$Q = mcp(Tout - Tin) \tag{7}$$

where m denotes the mass flow rate of air (kg/s), C_p represents the specific heat capacity of air (J/(kg · K)), T_{out} indicates the average outlet air temperature (K), and T_{in} represents the average inlet air temperature (K).

The calculation formula of ΔT[30]:

Boundary condition	Equation
Velocity-inlet	$\mathrm{u} = \mathrm{uin}, \mathrm{v} = \mathrm{w} = 0, \mathrm{Tin} = 308\mathrm{K}$
Outflow	$\frac{\partial \mathrm{u}}{\partial \mathrm{x}} = \frac{\partial \mathrm{v}}{\partial \mathrm{x}} = \frac{\partial \mathrm{w}}{\partial \mathrm{x}} = \frac{\partial \mathrm{T}}{\partial \mathrm{x}} = 0$
Symmetry	$\frac{\partial \mathrm{u}}{\partial \mathrm{z}} = \frac{\partial \mathrm{v}}{\partial \mathrm{z}} = \frac{\partial \mathrm{T}}{\partial \mathrm{z}} = 0, \mathrm{w} = 0$
Periodic	$\delta(\mathrm{z}) = \delta(\mathrm{z} + fp) = \delta(\mathrm{z} + 2fp), \delta$ is any value

Table 3. Boundary condition equations.

$$\Delta T = \frac{(Tin - Tw) - (Tout - Tw)}{In\frac{(Tin-Tw)}{(Tout-Tw)}} \tag{8}$$

where T_{in} denotes the average inlet air temperature (K), T_{out} denotes the average outlet temperature (K), and T_w corresponds to the wall temperature of the copper tube (K).

Heat transfer factor (j)[32,33]:

$$j = \frac{h}{\rho umcp} pr^{2/3} \tag{9}$$

where h denotes the convective heat transfer coefficient, u_m represents the inlet air velocity, and Pr corresponds to the Prandtl number.

Pressure drop (ΔP)[34]:

$$\Delta P = (Pin - Pout) \tag{10}$$

where P_{in} represents inlet air pressure and P_{out} indicates outlet air pressure (Pa).

Friction factor (f)[35]:

$$f = \frac{2\Delta PDc}{\rho u_m^2 L} \tag{11}$$

where ΔP represents pressure drop (Pa), and L represents the fin length along the airflow direction (m).

The thermal performance factor (JF) based on identical pump power is defined as follows[36]:

$$JF = \frac{(Nu/Nu_0)}{(f/f_0)^{1/3}} \tag{12}$$

where Nu denotes the Nusselt number of the FTHE with VGs, and Nu_0 denotes the Nusselt number of the FTHE without VGs. f represents the friction factor of the FTHE with VGs, and f_0 represents the friction factor of the FTHE without VGs.

Mesh generation and model validation

ANSYS Fluent Meshing was employed for mesh generation. A structured mesh scheme was adopted to enhance mesh quality and numerical convergence. The mesh model is illustrated in Fig. 3. To validate grid independence, simulations were performed with grid systems of varying resolutions while maintaining identical computational parameters. The results of grid independence test are presented in Fig. 4. As the grid number increased from 200,000 to 1,880,000, both Nu and f exhibited a downward trend, with maximum deviations of 1.7% and 3.0%, respectively.

Grid convergence index (GCI) is used to evaluate the mesh quality. GCI is defined as[37].

$$\mathrm{GCI} = \frac{1.25\mathrm{e}}{\mathrm{r^p} - 1} \tag{13}$$

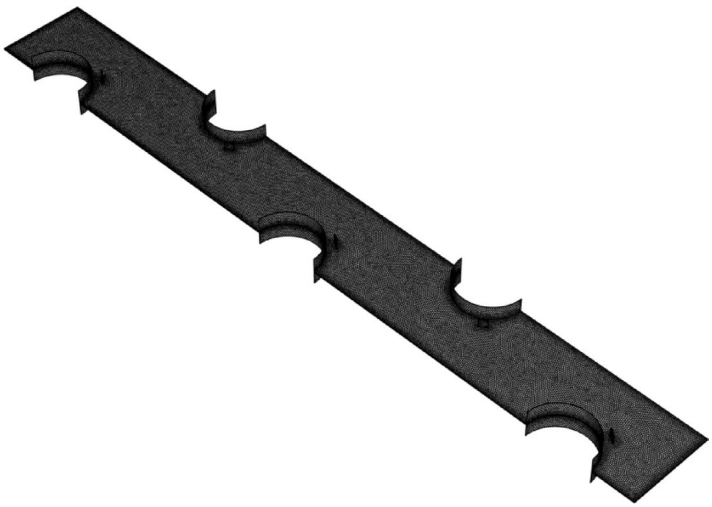

Fig. 3. Mesh model (this figure was created by the Fluent Meshing tool of ANSYS Fluent 2021R1).

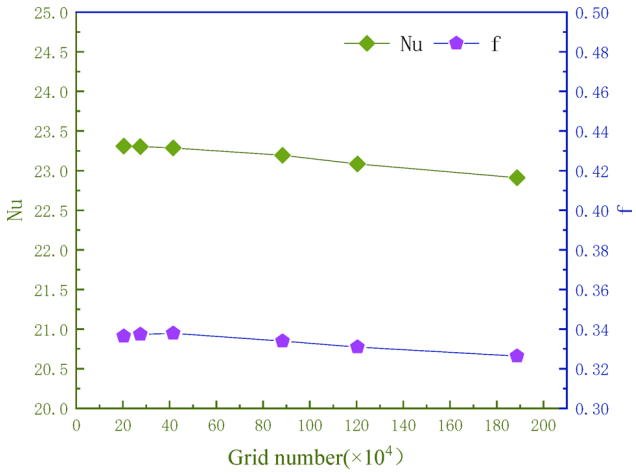

Fig. 4. Grid independence test.

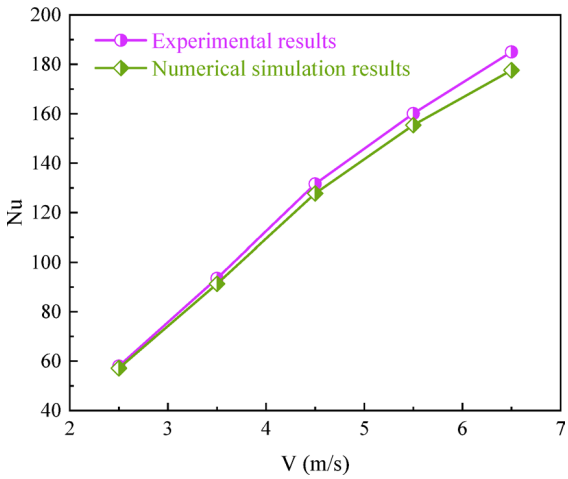

Fig. 5. Comparison of Nu.

where 1.25 is the safety factor, r is the mesh refinement rate, p is the order of convergence, and e is the relative error. The parameters of p, e, and r is expressed as:

$$\mathrm{p} = \frac{|\ln|(\phi_3 - \phi_2)/(\phi_2 - \phi_1)||}{\ln(\mathrm{r})} \tag{14}$$

$$\mathrm{e} = \left|\frac{\phi_1 - \phi_2}{\phi_1}\right| \tag{15}$$

$$\mathrm{r} = \frac{\mathrm{h_{coarse}}}{\mathrm{h_{fine}}} \tag{16}$$

$$\mathrm{h} = \left[\frac{1}{\mathrm{N}}\sum_{\mathrm{i}=1}^{\mathrm{N}}(\Delta \mathrm{V}_i)\right]^{1/3} \tag{17}$$

whereϕ_1,ϕ_2,and$\phi_3$represent numerical solutions of coarse, medium, and fine meshes, respectively. The number of coarse, medium, and fine grids selected were 274,495, 883,417, and 1,886,695, respectively. The calculated GCI for the outlet temperature was 0.0037, indicating that the mesh quality of the model is satisfactory. To balance computational efficiency and accuracy, the number of grids was selected to be 1,200,000 for subsequent simulations.

To verify the accuracy of the numerical simulation results, a three-dimensional computational model was developed according to the dimensions of the experimental fin[38]. The comparison between the numerical simulation and the experimental results, shown in Figs. 5 and 6, revealed maximum relative errors of 4.2%

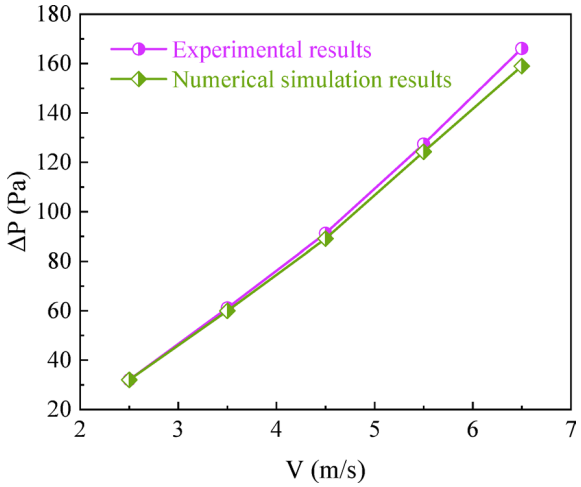

Fig. 6. Comparison of ΔP.

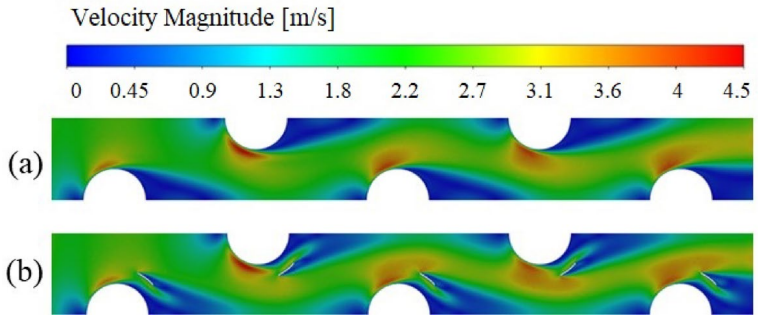

Fig. 7. The influence of VGs on the air velocity field (a) without VG, (b) with VG.

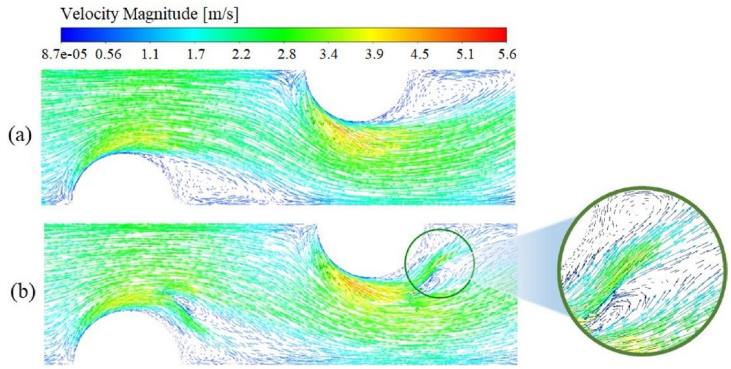

Fig. 8. Air velocity vector diagram (**a**) without VG, (**b**) with VG.

for Nu and 4.5% for ΔP. These discrepancies indicate that the model accurately reflects the fluid flow and heat transfer, thereby confirming the reliability of the physical model's calculation.

Results and discussion

Effects of VG on the velocity field

The simulation parameters were configured as follows: $\alpha = 40°$, $\beta = 40°$, $\theta = 25°$, and $H = 1.2$ mm. Figure 7 illustrates the influence of VGs on the air velocity field at an airflow velocity ($V = 2.0$ m/s). Without VGs, the airflow exhibited stable behavior with uniform velocity distribution. The airflow was deflected into the wake region downstream of the copper tube upon VG installation. Figure 8 displays the velocity vector distribution at $V = 2.0$ m/s, showing an intensified velocity gradient near the VGs that indicates localized airflow acceleration.

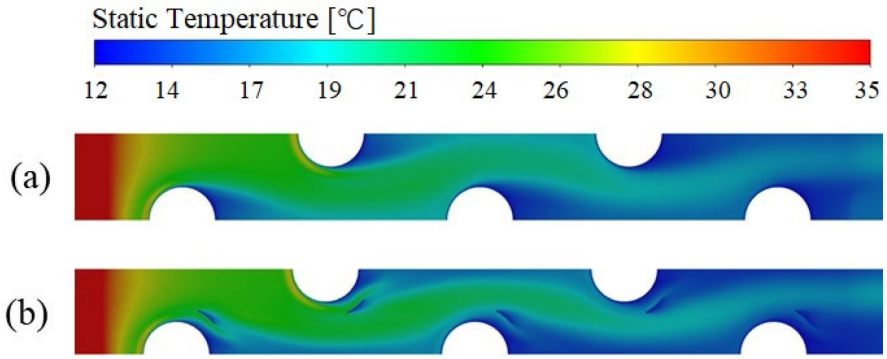

Fig. 9. The effect of VGs on temperature field (**a**) without VG, (**b**) with VG.

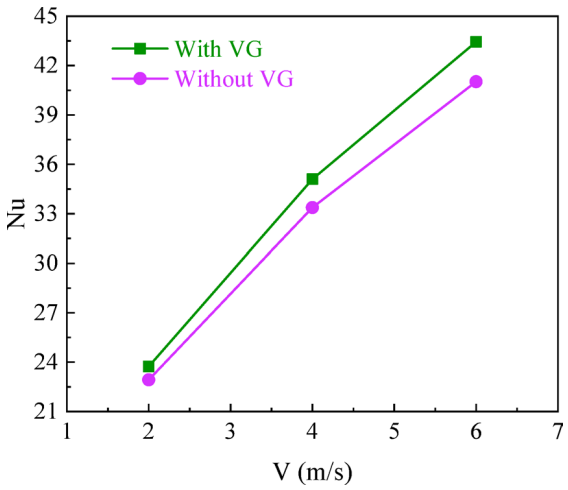

Fig. 10. Relationship between V and Nu.

Under the condition of without VG, distinct low-velocity regions and dispersed streamline distributions were observed in the copper tube wake region, consistent with previous findings[39]. In contrast, VGs significantly enhanced turbulent mixing, thereby reducing the thermally inefficient region.

Influence of VG on the temperature field

Figure 9 compares the temperature fields with and without VGs. Without VGs, the temperature distribution remained uniform, whereas localized temperature gradients developed with VGs installation. Figure 10 demonstrates the correlation between the Nu and V. At V = 6.0 m/s, the Nu value for the FTHE with VGs was 5.9% higher than that of without VGs. The Nu values increased with the increase of V, indicating that higher airflow velocities significantly enhance convective heat transfer coefficient. Notably, the Nu values with VGs consistently surpassed those without VGs, demonstrating that VGs improve thermal performance through enhanced turbulent mixing.

The influence of VG size on temperature field and velocity field

Effects of θ on the performance of FTHE

The simulation parameters for the VGs were configured as follows: H = 1.2 mm, α = 50°, β = 30°, and V = 6.0 m/s. The influence of θ on the temperature and velocity fields is shown in Fig. 11. It can be seen that the air temperature distribution is relatively uniform at θ = 10°, with no distinct high- or low-temperature regions observed downstream of the third row of copper tubes. The high-temperature regions gradually expand as θ increases. Simultaneously, the high-velocity regions progressively intensify with increasing θ, resulting from airflow channel narrowing.

Table 4 summarizes the influence of θ on the thermal performance of FTHEs. All three parameters j, f, and JF demonstrate monotonic enhancement with increasing θ. This trend is attributed to the extended chord length of VGs at larger θ values, which amplifies vortex intensity[40]. The elevation of θ strengthens vortical motion during airflow through FTHEs, consequently enhancing the local heat transfer coefficient. The JF values exceeding 1.0 across the θ range of 10°–35°. At θ = 35°, JF and f showed respective increases of 5.2% and 23.3% compared to the baseline configuration without VGs. These results indicate that larger θ values enhances heat transfer efficiency.

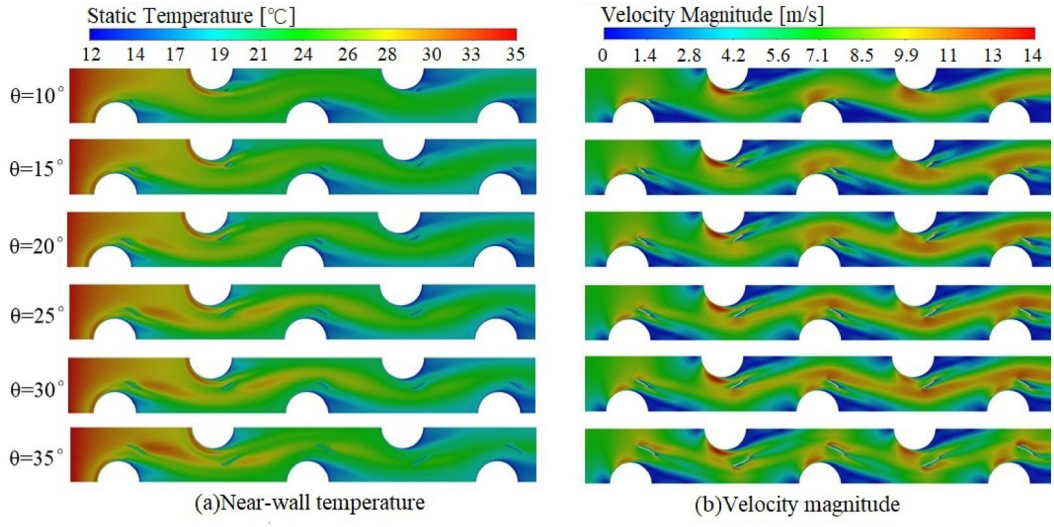

Fig. 11. Influence of θ on temperature field and velocity field.

θ(°)	j(×10^{-2})	f	JF
0	0.764	0.231	1.0
10	0.762	0.233	0.995
15	0.783	0.249	0.999
20	0.801	0.255	1.016
25	0.828	0.266	1.036
30	0.830	0.268	1.036
35	0.860	0.285	1.052

Table 4. The influence of θ on the thermal performance of FTHEs.

However, shear-driven interactions between high- and low-velocity zones create complex flow patterns, resulting in elevated pressure losses and potential mechanical fatigue risks in the heat exchanger.

Effects of H on the performance of FTHE

The simulation parameters for the VGs were configured as follows: α = 50°, β = 30°, θ = 25°, and V = 6.0 m/s. Figure 12 illustrates the influence of H on temperature and velocity fields. At H = 0.4 mm, the FTHEs surface exhibited uniform temperature distribution. The number of high-temperature regions increased with the increase of H, and the temperature distribution became non-uniform when H > 1.0 mm.

Figure 13 displays the vorticity distribution on the X-axis cross-sectional plane downstream of the first copper tube column. Under the condition of without VGs (H = 0), both fluid vorticity and vortex extent were minimal. The addition of VGs significantly increase the vorticity and vortex range. The disturbance effect of VGs intensified with rising H, enhancing convective heat transfer coefficient. However, when H > 1.0 mm, complex flow patterns emerged due to multiple high-velocity regions, suggesting a trade-off between heat transfer enhancement and flow stability.

Table 5 summarizes the impact of different height on the thermal performance of FTHEs. When H increases from 0 to 0.6 mm, the JF factor declines, indicating inadequate thermal coupling between airflow and FTHEs. Beyond H = 0.8 mm, both j and JF rise monotonically, peaking at H = 1.6 mm with j and f increasing by 13.0% and 24.7%, respectively, compared to the baseline configuration without VGs. This trend is attributed to enhanced convective heat transfer across copper tube surfaces and intensified vortical flow of air. However, the concurrent increase in f highlights a trade-off between heat transfer enhancement and pressure loss. These findings conclusively demonstrate that H must exceed 0.8 mm to achieve net performance improvements in FTHE systems.

Effects of α and β on the performance of FTHE

The angle between VGs and the airflow is an important parameter that influences VG's fluid guidance[41]. Therefore, the effects of α and β on FTHEs are further studied. Numerical simulations were performed with parameters set to θ = 25°, H = 1.2 mm, and V = 6.0 m/s. Figure 14 reveals the influence of α on temperature field and velocity field: uniform temperature distribution prevailed at α < 30°, while localized high-temperature

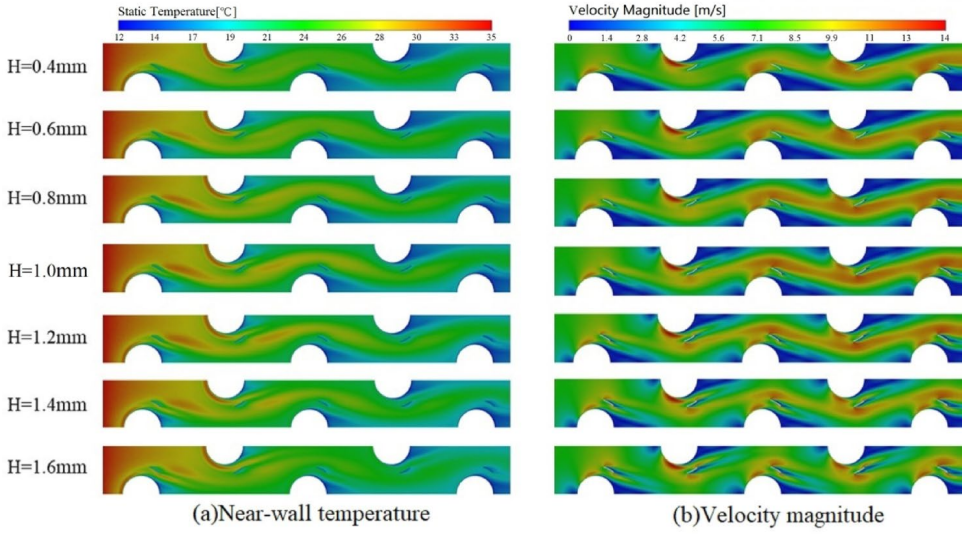

Fig. 12. The influence of H on temperature field and velocity field.

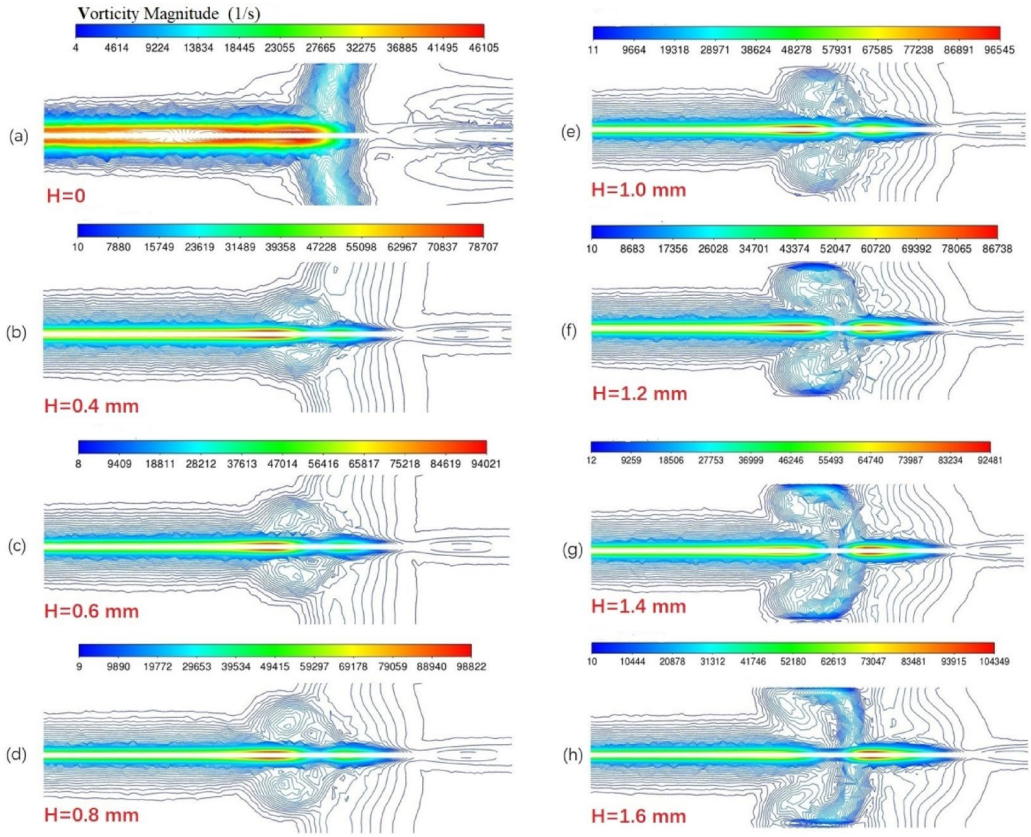

Fig. 13. Contour plots of vorticity.

regions emerged when α exceeded 45°. Simultaneously, intermittent high-velocity regions expanded with rising α values, eventually forming continuous banded structures.

Figure 15 shows the influence of β on temperature and velocity fields. Uniform temperature distribution is observed at β = 25°, while the wake region downstream of the copper tube diminishes progressively with increasing β, consistent with the previous research[42]. Elevated β values enlarge the airflow channel area, expanding high-temperature regions and augmenting local convective heat transfer. Concurrently, intensified turbulence at higher β amplifies high-velocity regions.

H(mm)	j(×10^{-2})	f	JF
0	0.764	0.231	1
0.4	0.759	0.235	0.986
0.6	0.769	0.241	0.982
0.8	0.792	0.249	1.011
1	0.814	0.258	1.028
1.2	0.829	0.267	1.036
1.4	0.84	0.276	1.038
1.6	0.863	0.288	1.052

Table 5. The impact of different height on the thermal performance of FTHEs.

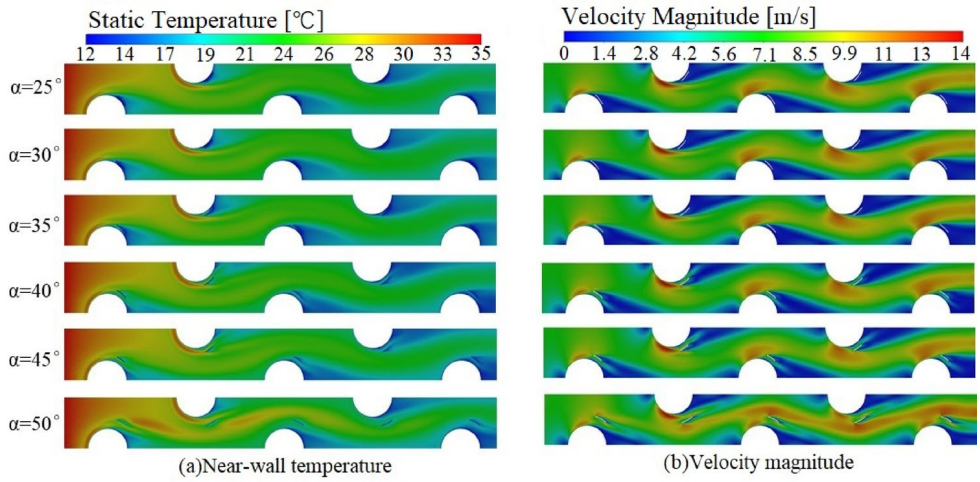

Fig. 14. The influence of α on temperature field and velocity field.

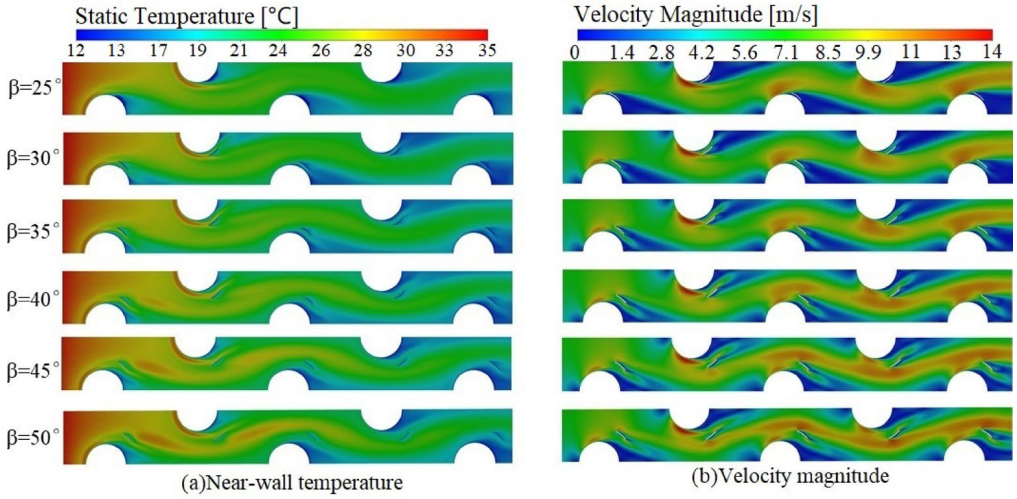

Fig. 15. Influence of β on temperature field and velocity field.

Effects of α and β on the performance of FTHEs are shown in Fig. 16. The value of j initially decreased and subsequently increased with rising α, whereas it exhibited a monotonic increase with β, demonstrating the superiority of higher β values for heat transfer enhancement. The value of f increased with both α and β, indicating that larger angles lead to elevated flow resistance caused by VG-induced airflow obstruction. JF declined as α increased from 25° to 35°, then rose with further increases in α. At α = 50°, j and f increased by

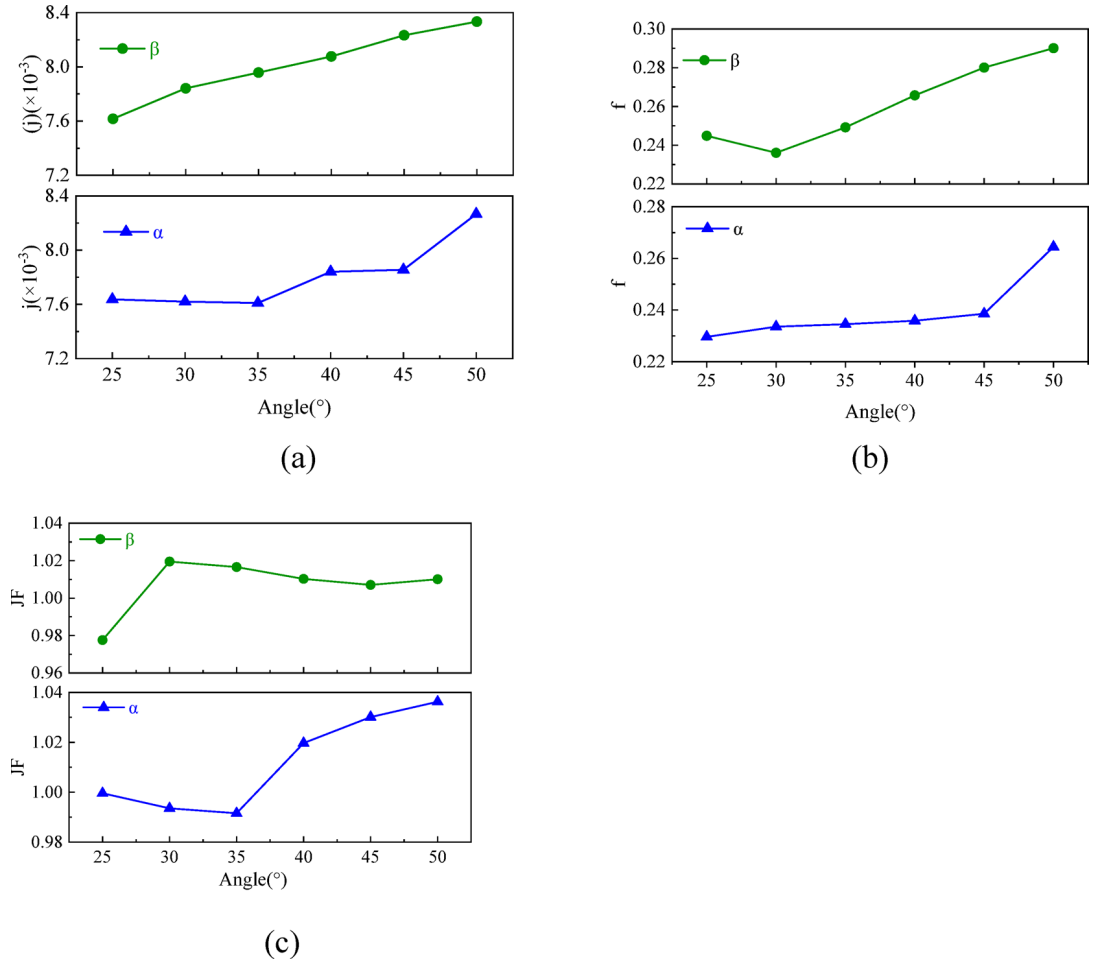

Fig. 16. Effects of α and β on the performance of FTHEs.

8.2% and 14.5%, respectively. Similarly, JF first rose then fell with β but remained above 1.0, peaking at β = 30° with 2.0% and 2.2% increases in JF and f. These trends are explained by VGs positioning effects. For α < 35°, VGs primarily occupy the thermally inefficient wake region behind copper tubes, whereas at α > 35°, direct VG-airflow interaction enhances turbulence and local heat transfer.

Conclusions

This study investigates the impact of circular arc VGs on the heat transfer and hydrodynamic performance of FTHEs through numerical simulations. A systematic analysis is conducted to evaluate the effects of key geometric parameters on heat transfer enhancement and flow resistance characteristics in FTHEs. The key findings are summarized as follows:

1. Circular arc VGs significantly enhance the thermal performance of FTHEs by generating longitudinal vortices that disrupt boundary layers and intensify turbulence. At an airflow velocity of 6.0 m/s, the Nu for VG-equipped FTHEs exceeded non-VG configurations by 5.9%, validating the efficacy of vortex-driven heat transfer. Larger θ values strengthen vorticity, improving both j and JF. At θ = 35°, JF increased by 5.2%.
2. A critical threshold of H ≥ 0.8 mm was identified for optimal performance. When H increases from 0.8 to 1.6 mm, compared with FTHE without VGs, the j and f of FTHE with VGs increase by 13.0% and 24.7% respectively.
3. When α = 25°–35°, VGs exhibited negligible heat transfer enhancement in FTHE. However, for α = 35°–50°, VGs significantly improved heat transfer performance, with j and f increasing by 8.2% and 14.5%, respectively, at α = 50°. Similarly, higher β value is beneficial to enhance convective heat transfer, achieving 2.0% and 2.2% improvements in JF and f at β = 30°.

The study establishes a trade-off between heat transfer enhancement and pressure drop, emphasizing the need for balanced geometric optimization. These results serve as a foundation for energy-efficient FTHE designs in refrigeration and HVAC applications.

Data availability

The data that support the findings of this study are available from the corresponding author upon reasonable request.

Received: 16 January 2025; Accepted: 30 May 2025
Published online: 01 July 2025

References

1. Marzouk, S. A., Almehmadi, F. A., Aljabr, A. T., Alam, T. & Singh R.Khargotra, effects of extended pin fins on the hydrothermal performance of double pipe heat exchanger. *Therm. Sci. Eng. Prog.* **55**, 102915 (2024).
2. Marzouk, S. A. et al. Numerical and experimental investigation of heat transfer enhancement in double tube heat exchanger using nail rod inserts. *Sci. Rep.* **14**, 9637. https://doi.org/10.1038/s41598-024-59085-5 (2024).
3. Marzouk, S. A., Abou Al-Sood, M., El-Said, E. M. & Younes, M. El-Fakharany,Evaluating the effects of bifurcation angle on the performance of a novel heat exchanger based on contractual theory. *Renew. Energ.* **219**, 119463. https://doi.org/10.1016/j.renene.2023.119463 (2023).
4. Tao, W. Q., Cheng, Y. P. & Lee, T. S. 3D numerical simulation on fluid flow and heat transfer characteristics in multistage heat exchanger with Slit fins. *Heat Mass Transf.* **44** (1), 125–136. https://doi.org/10.1007/s00231-006-0227-2 (2007).
5. Lu, G. & Zhou, G. Numerical simulation on performances of plane and curved winglet type vortex generator pairs with punched holes. *Int. J. Heat Mass Transf.* **102**, 679–690. https://doi.org/10.1016/j.ijheatmasstransfer.2016.06.063 (2016).
6. Kang, H., Li, W., Li, H., Xin, R. & Tao, W. Experimental study on heat transfer and pressure drop characteristics of four types of plate fin-and-tube heat exchanger surfaces. *J. Therm. Sci.* **3** (1), 34–42. https://doi.org/10.1007/BF02653243 (1994).
7. Ouyang, X. & Hu, H. Simulation study on optimal structure of circular corrugated finned tube. *Int. J. Therm. Sci.* **179**, 107622. https://doi.org/10.1016/j.ijthermalsci.2022.107622 (2022).
8. Habibian, S. H., Abolmaali, M., Afshin, A. & H Numerical investigation of the effects of fin shape, antifreeze and nanoparticles on the performance of compact finned-tube heat exchangers for automobile radiator. *Appl. Therm. Eng.* **133**, 248–260. https://doi.org/10.1016/j.applthermaleng.2018.01.032 (2018).
9. Johnson, T. R. & Joubert, P. N. The influence of Vortex generators on the drag and heat transfer from a circular cylinder normal to an airstream. **91**, 91–99. (1969).
10. Fiebig, M. Vortices, generators and heat transfer. *Chem. Eng. Res. Des.* **76** (2), 108–123. https://doi.org/10.1205/026387698524686 (1998).
11. Modi, A. J. & Rathod, M. K. Experimental investigation of heat transfer enhancement and pressure drop of fin-and-circular tube heat exchangers with modified rectangular winglet vortex generator. *Int. J. Heat Mass Transf.* **189**, 122742. https://doi.org/10.1016/j.ijheatmasstransfer.2022.122742 (2022).
12. Han, Z., Xu, Z. & Wang, J. Numerical simulation on heat transfer characteristics of rectangular vortex generators with a hole. *Int. J. Heat Mass Transf.* **126**, 993–1001. https://doi.org/10.1016/j.ijheatmasstransfer.2018.06.081 (2018).
13. Leu, J. S., Wu, Y. H. & Jang, J. Y. Heat transfer and fluid flow analysis in plate-fin and tube heat exchangers with a pair of block shape vortex generators. *Int. J. Heat Mass Transf.* **47** (19), 4327–4338. https://doi.org/10.1016/j.ijheatmasstransfer.2004.04.031 (2004).
14. Allison, C. B. & Dally, B. B. Effect of a delta-winglet vortex pair on the performance of a tube–fin heat exchanger. *Int. J. Heat Mass Transf.* **50** (25), 5065–5072. https://doi.org/10.1016/j.ijheatmasstransfer.2007.08.003 (2007).
15. Lotfi, B., Sundén, B. & Wang, Q. An investigation of the thermo-hydraulic performance of the smooth wavy fin-and-elliptical tube heat exchangers utilizing new type vortex generators. *Appl. Energy.* **162**, 1282–1302. https://doi.org/10.1016/j.apenergy.2015.07.065 (2016).
16. Zheng, S. et al. Numerical investigation on thermal–hydraulic characteristics in a mini-channel with trapezoidal cross-section longitudinal vortex generators. *Appl. Therm. Eng.* **205**, 118004. https://doi.org/10.1016/j.applthermaleng.2021.118004 (2022).
17. Lin, Z., Liu, C., Lin, M. & Wang, L. Numerical study of flow and heat transfer enhancement of circular tube bank fin heat exchanger with curved delta-winglet vortex generators. *Appl. Therm. Eng.* **88**, 198–210. https://doi.org/10.1016/j.applthermaleng.2014.11.079 (2015).
18. Zhou, G. & Ye, Q. Experimental investigations of thermal and flow characteristics of curved trapezoidal winglet type vortex generators. *Appl. Therm. Eng.* **37**, 241–248. https://doi.org/10.1016/j.applthermaleng.2011.11.024 (2012).
19. Esmaeilzadeh, A., Amanifard, N. & Deylami, H. M. Comparison of simple and curved trapezoidal longitudinal vortex generators for optimum flow characteristics and heat transfer augmentation in a heat exchanger. *Appl. Therm. Eng.* **125**, 1414–1425. https://doi.org/10.1016/j.applthermaleng.2017.07.115 (2017).
20. Song, K. et al. Effect of geometric size of curved delta winglet vortex generators and tube pitch on heat transfer characteristics of fin-tube heat exchanger. *Exp. Thermal Fluid Sci.* **82**, 8–18. https://doi.org/10.1016/j.expthermflusci.2016.11.002 (2017).
21. Naik, H., Harikrishnan, S. & Shaligram, T. Numerical investigations on heat transfer characteristics of curved rectangular winglet placed in a channel. *Int. J. Therm. Sci.* **129**, 489–503. https://doi.org/10.1016/j.ijthermalsci.2018.03.028 (2018).
22. Oh, Y. & Kim, K. Effects of position and geometry of curved vortex generators on fin-tube heat-exchanger performance characteristics. *Appl. Therm. Eng.* 189116736. https://doi.org/10.1016/j.applthermaleng.2021.116736 (2021).
23. Fiebig, M., Mitra, N. K. & Dong, Y. M. Simultaneous heat transfer enhancement and flow loss reduction of fin-tubes. (1990).
24. Biswas, G., Mitra, N. K. & Fiebig, M. Heat transfer enhancement in fin-tube heat exchangers by winglet type vortex generators. *Int. J. Heat Mass Transf.* **37** (2), 283–291. https://doi.org/10.1016/0017-9310(94)90099-X (1994).
25. Gholami, A., Wahid, M. A. & Mohammed, H. A. Thermal–hydraulic performance of fin-and-oval tube compact heat exchangers with innovative design of corrugated fin patterns. *Int. J. Heat Mass Transf.* **106**, 573–592. https://doi.org/10.1016/j.ijheatmasstransfer.2016.09.028 (2017).
26. Behfard, M. & Sohankar, A. Numerical investigation for finding the appropriate design parameters of a fin-and-tube heat exchanger with delta-winglet vortex generators. *Heat Mass Transf.* **52** (1), 21–37. https://doi.org/10.1007/s00231-015-1705-1 (2016).
27. Saini, P. & Shah, M. P. Performance evaluation of finned tube heat exchanger using curved wavy delta winglet vortex generators with circular perforations. *Int. Commun. Heat. Mass. Transf.* **159**, 108184 (2024).
28. Qu, Z. G., Tao, W. Q. & He, Y. L. Three-Dimensional numerical simulation on laminar heat transfer and fluid flow characteristics of strip fin surface with X-Arrangement of strips. Journal of heat transfer-transactions of the Asme. *J. Heat Transfer.* **126**. https://doi.org/10.1115/1.1798971 (2004).
29. Van Doormaal, J. P. & Raithby, G. D. Enhancement of the simple method for predicting incompressibile fluid flows. *Numer. Heat. Transf.* **7** (2), 147–163. https://doi.org/10.1080/01495728408961817 (1984).
30. Saini, P., Dhar, A. & Powar, S. Performance enhancement of fin and tube heat exchanger employing curved trapezoidal winglet vortex generator with circular punched holes. *Int. J. Heat Mass Transf.* **209**, 124142. https://doi.org/10.1016/j.ijheatmasstransfer.2023.124142 (2023).
31. Sharaf, M. A. et al. Effects of multi-spring wires on hydrothermal performance of double tube heat exchanger. *Case Stud. Therm. Eng.* **60**, 104689 (2024).

32. Modi, A. J., Kalel, N. A. & Rathod, M. K. Thermal performance augmentation of fin-and-tube heat exchanger using rectangular winglet vortex generators having circular punched holes. *Int. J. Heat Mass Transf.* **158**, 119724. https://doi.org/10.1016/j.ijheatmasstransfer.2020.119724 (2020).
33. Moreno, R. R., Pérez, A. M. & Pérez, R. B. Numerical optimization of a heat exchanger with Slit fins and vortex generators using genetic algorithms. *Int. J. Refrig.* **119**, 247–256. https://doi.org/10.1016/j.ijrefrig.2020.07.023 (2020).
34. Ashish, J., Modi, Navnath, A. K. & Manish, K. R. Thermal performance aug-mentation of fin-and-tube heat exchanger using rectangular winglet vortex generators having circular punched holes. *Int. J. Heat. Mass. Transf.* **158**, 119724 (2020).
35. Zeng, M., Tang, L. H., Lin, M. & Wang, Q. Optimization of heat exchangers with vortex-generator fin by Taguchi method. *Appl. Therm. Eng.* **30** (13), 1775–1783. https://doi.org/10.1016/j.applthermaleng.2010.04.009 (2010).
36. Shah, R. K. Compact heat exchanger surface selection methods. (1978).
37. Procedure for Estimation. And reporting of uncertainty due to discretization in CFD applications. ASME. *J. Fluids Eng. July*. **130** (7), 078001 (2008).
38. Wu, Z., Xiang, L. & Lin, F. Study on heat transfer performance and pressure drop characteristics of flat-fin tube heat exchanger. *Shanxi Archit.* **45** (12), 91–93. https://doi.org/10.13719/j.cnki.cn14-1279/tu.2019.12.051 (2019). (in chinese).
39. Lemouedda, A., Breuer, M., Franz, E., Botsch, T. & Delgado, A. Optimization of the angle of attack of delta-winglet vortex generators in a plate-fin-and-tube heat exchanger. *Int. J. Heat Mass Transf.* **53** (23), 5386–5399. https://doi.org/10.1016/j.ijheatmasstransfer.2010.07.017 (2010).
40. Lu, G. & Zhai, X. Effects of curved vortex generators on the air-side performance of fin-and-tube heat exchangers. *Int. J. Therm. Sci.* **136**, 509–518. https://doi.org/10.1016/j.ijthermalsci.2018.11.009 (2019).
41. Luo, C., Wu, S., Song, K., Hua, L. & Wang, L. Thermo-hydraulic performance optimization of wavy fin heat exchanger by combining delta winglet vortex generators. *Appl. Therm. Eng.* **163**, 114343. https://doi.org/10.1016/j.applthermaleng (2019).
42. Batista, J., Trp, A., Lenic, K. & Kirincic, M. The influence of geometry parameters of rectangular vortex generators on the air-to-water fin-and-tube heat exchanger efficiency enhancement. *Int Commun Heat Mass Transf Mar* **162** 108647. https://doi.org/10.1016/J.ICHEATMASSTRANSFER (2025).

Author contributions

X.Q. contributed to writing and editing. J.Y. contributed to writing original draft and investigation. Y.Z.contributed to editing. J.W. contributed to methodology. X.G. contributed to investigation. All authors have given approval to the final version of the manuscript.

Declarations

Competing interests

The authors declare no competing interests.

Additional information

Correspondence and requests for materials should be addressed to X.Q.

Reprints and permissions information is available at www.nature.com/reprints.

Publisher's note Springer Nature remains neutral with regard to jurisdictional claims in published maps and institutional affiliations.